Talanta 296 (2026) 128449

Contents lists available at ScienceDirect

Talanta

journal homepage: www.elsevier.com/locate/talanta

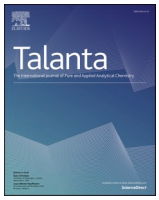

Chemiluminescent semiconductor polymer nanoparticles for sensitive H_2O_2 detection based on chemiluminescence resonance energy transfer

Ximin Mai, Jiahui Li, Pinyi Ma, Daqian Song, Qiang Fei *

College of Chemistry, Jilin Province Research Center for Engineering and Technology of Spectral Analytical Instruments, Jilin University, Qianjin Street 2699, Changchun, 130012, China

ARTICLE INFO

Keywords:
Chemiluminescence resonance energy transfer (CRET)
Semiconductor polymer nanoparticles (SPNs)
Chemiluminescence (CL)
Hydrogen peroxide (H_2O_2)

ABSTRACT

In this work, a novel chemiluminescent semiconducting polymer nanoparticles PFBT-ABEI-PEG (PAP SPNs) has been designed and synthesized, which consisted of poly(9,9-dioctylfluorene-alt-benzothiadiazole) (PFBT) main chains, N-(4-Aminobutyl)-N-ethylisoluminol (ABEI) and Polyethylene glycol (PEG) side chains conjugated. Through the exploration of covalent linkage and optimal conformation, the distance between donor-acceptor molecules has been considerably shortened, thereby greatly enhancing the efficiency of chemiluminescence resonance energy transfer (CRET). Hydrogen peroxide (H_2O_2) is both a key signaling molecule and an important regulator of redox balance, playing dual roles in a variety of pathophysiological processes. We established a stable intramolecular CRET system based on PAP SPNs, which showed highly sensitive response to H_2O_2. The limit of detection can reach as low as 33.88 nM under the optimum experimental conditions. Finally, this method was successfully applied to the detection of H_2O_2 in cancer cells.

1. Introduction

Reactive oxygen species (ROS) is an unstable, highly reactive, and partially reduced oxygen derivative produced during cellular metabolism. ROS are both a key signaling molecule and an important mediator of oxidative damage, which totally include hydrogen peroxide (H_2O_2) [1], superoxide anion ($O_2^{\bullet-}$) [2], hypochlorous acid(HOCl) [3], singlet oxygen ($^1O_2$) [4], and hydroxyl radical (•OH) [5]. Dysregulation of ROS signaling can severely affect the pathophysiology of disease, especially playing a key role in cellular metabolism and inflammatory signaling [6]. Under the normal cellular circumstances, the oxidative and antioxidant systems within the cell can effectively balance each other, with antioxidants clearing excess oxidants to maintain a stable and balanced cellular environment [7]. However, when the cell is subjected to harmful stimuli, the equilibrium of the intracellular oxidation-reduction process is disrupted, which affects biomacromolecules, such as DNA, RNA, and proteins, as well as lipids [8,9]. Once these biomolecules are damaged, resulting in the continuous accumulation of a substantial quantity of oxidative intermediates, it may lead to either cell death or the promotion of malignant transformation into cancer cells [10]. The overproduction of major ROS produced in organisms has been closely associated with the onset and progression of a variety of diseases, including cancer, arthritis, chronic obstructive pulmonary disease, and neurodegenerative diseases [11].

Chemiluminescence (CL) is a phenomenon of light radiation that accompanies a substance during a chemical reaction [4,12–14]. Chemiluminescence resonance energy transfer (CRET) is defined as an optical process which involving the non-radiative dipole-dipole transfer of energy from the excited state donor molecule to a fluorescent or non-fluorescent energy acceptor molecule by chemical reaction [15]. In addition, CRET has exhibited plenty of advantages compared with other resonance energy transfer, it does not require additional light source, which refrains from the influence about stray light as well as instability of light source and succeed in chemiluminescence detection with neglectable background noise [15–17]. As the recent arrival of the era of continuous advancement of nanoscience and nanotechnology, nanomaterials have garnered considerable attention in the realm of CRET due to their numerous exceptional properties, encompassing graphene and graphene oxide [18,19], quantum dots [20,21], covalent organic frameworks [12], semiconductor polymer nanoparticles [4,22], metal organic frameworks [13,14], precious metal nanoparticles [23], and transition metal nanomaterials [24], among others. Semiconducting polymer nanoparticles (SPNs) as a chemiluminescence receptor possess a lot of outstanding advantages, including high fluorescence quantum

* Corresponding author.
E-mail address: feiqiang@jlu.edu.cn (Q. Fei).

https://doi.org/10.1016/j.talanta.2025.128449
Received 7 April 2025; Received in revised form 26 May 2025; Accepted 7 June 2025
Available online 7 June 2025

yield, excellent photostability biocompatibility as well as sensing ability, large extinction coefficients and easy surface modification [25–28]. Therefore, they are widely used as a chemiluminescence energy receptor and apply to photodynamic therapy (PDT) and biological imaging analysis for the diagnosis and treatment of diseases [26,27,29].

In this work, a novel semiconductor polymer nanoparticles PFBT-ABEI-PEG (PAP) was designed and synthesized, which consists of Poly [(9,9-di-*n*-octylfluorenyl-2,7-diyl)-alt-(benzo [1–3] thiadia-zol-4, 8-diyl)] (PFBT) main chain, N-(4-Aminobutyl)-N-ethylisoluminol (ABEI) side chain, and Polyethylene glycol (PEG). The side chain ABEI fulfils the roles of both a responsive unit for H_2O_2 and an energy donor, while the main chain (PFBT) serves as both a photosensitizer and an energy acceptor. PFBT can be excited by blue light at around 460 nm emitted by ABEI oxidation, thereby enabling the generation of chemiluminescence signals without the requirement for external light sources. Meanwhile, the different morphologies of semiconductor polymer nanoparticles were investigated by introducing polyethylene glycol (PEG) long chains, which improved the CRET efficiency and chemiluminescent stability of SPNs. Therefore, a self-supplied and highly sensitive CRET system based on PAP SPNs was successfully developed for the accurate detection of intracellular H_2O_2Fig. 1. In summary, the CRET assay system developed in this study not only simplifies the detection process, but also improves the sensitivity and reliability of the assay, which provides an important scientific tool and application prospect for the study of cancer-related diseases.

2. Result and discussion

2.1. Characterization of PAP SPNs

The hydrodynamic diameters of 0.5 mg/mL PFBT-ABEI, 0.5 mg/mL PAP SPNs and 5 mg/mL PAP SPNs were measured by dynamic light scattering (DLS), and the results indicating a maximum size of them approximately 67.86 nm, 147.07 nm and 189.23 nm (Fig. 2A–C). The slight discrepancy between the DLS and TEM measurements can be attributed to the shrinkage of the nanoparticles during the sample preparation for TEM. Compared with PFBT-ABEI (Fig. 2D), PAP SPNs are dense aggregates composed of many semiconductor polymer nanoparticles (Fig. 2F). The semiconductor polymer nanoparticles are tightly intertwined with each other by long chains of PEG, which shortens the intermolecular distances considerably. Regardless of the concentration of PAP SPNs, the addition of PEG resulted in a significant reduction of the intermolecular distance. It can be deduced that the formation of PAP SPNs is achieved through the amide bonds covalent linkage of ABEI and PFBT by FT-IR spectrum in Fig. S1. Therefore, PAP SPNs can generate chemiluminescence signals without an external light source via the intramolecular CRET [1,15,27]. After two months of storage at 4 °C in conditions of darkness, no precipitation was observed and CL intensity reached at least twofold that of the enhancer-free state, and the duration of the chemiluminescence was observed to increase sixfold compared with enhancer-free state (Fig. 6C). of PAP SPNs were essentially unchanged. This finding indicates that the SPNs exhibit remarkable stability in aqueous solution environment (Fig. S2).

2.2. Optimization of Synthetic conditions

In order to systematically optimize the chemiluminescence performance of PAP SPNs, the effects of PEG modification ratio and covalent coupling concentration on the luminescence properties were investigated. As shown in Fig. 3A, PEG feed ratio experiments showed that CL intensity was significantly enhanced in the range of 0–2 w/v%, while the enhancement increased gently in the range of 2–5 w/v%. Not only the hydrophilicity of PEG-encapsulated nanoparticles is enhanced [30,31], but also the distance between the molecules is greatly shortened (Fig. 2D and E), which directly leads to an improvement in the efficiency of CRET. ABEI concentration gradient experiments showed (Fig. 3B) that CL intensity increased continuously with increasing concentration in the interval of 0–5 mM, and reached a stable plateau period when the feed concentration was more than 5 mM, which indicating that the PAP SPNs had reached the saturated binding state. Combined all figures of Figs. 2 and 3, PFBT-ABEI and PAP SPNs (PFBT feeding concentration <0.5 mg/mL) molecularly dispersed and did not form a stable aggregation state. The zeta potential of them were greater than −30mV (Fig, S3).

According to the above experimental results, it is indicated that a single acceptor molecule not only efficiently accepts the energy transfer from covalently linked donor molecules, but also efficiently collides with the donor molecules in the solution; secondly, the increase in intermolecular distance reduces the non-radiation competitive pathways for energy transfer. The synergistic effect of these factors results in a system that exhibited anomalous light intensity enhancement properties in the low feeding concentration range of PFBT and direct reaction of PFBT-COOH with ABEI. The disordered random motion properties of molecules lead to a dynamic random collision pattern of donor-acceptor, and this intermolecular CRET is significantly stronger than intramolecular CRET, which in turn induces spatial heterogeneity in CRET efficiency. It essentially caused a significant decrease in the stability of CRET, significant fluctuations in signal strength and reduced experimental reproducibility. When the PFBT feeding concentration increased to 0.5 mg/mL (Fig. 3C), the CL intensity entered a stable plateau period. Increasingly, monodisperse nanoparticles are transformed to be

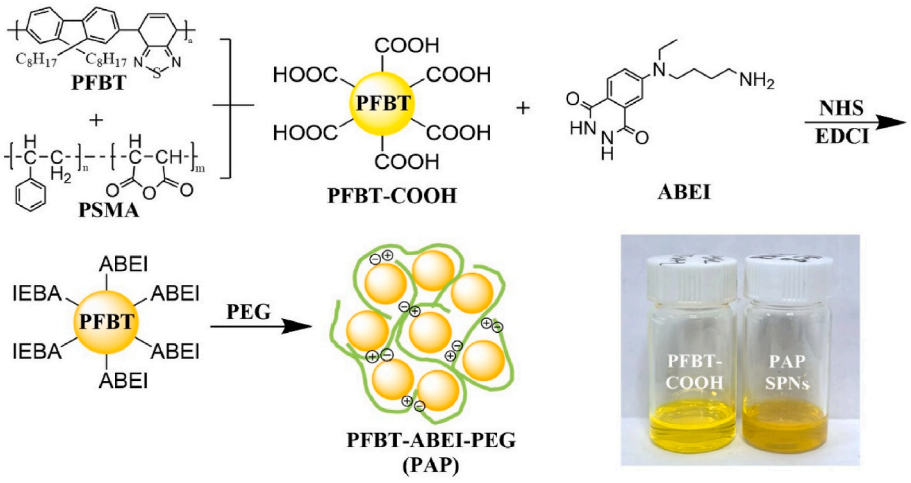

Fig. 1. Preparation of PFBT-COOH and chemiluminescent PAP SPNs.

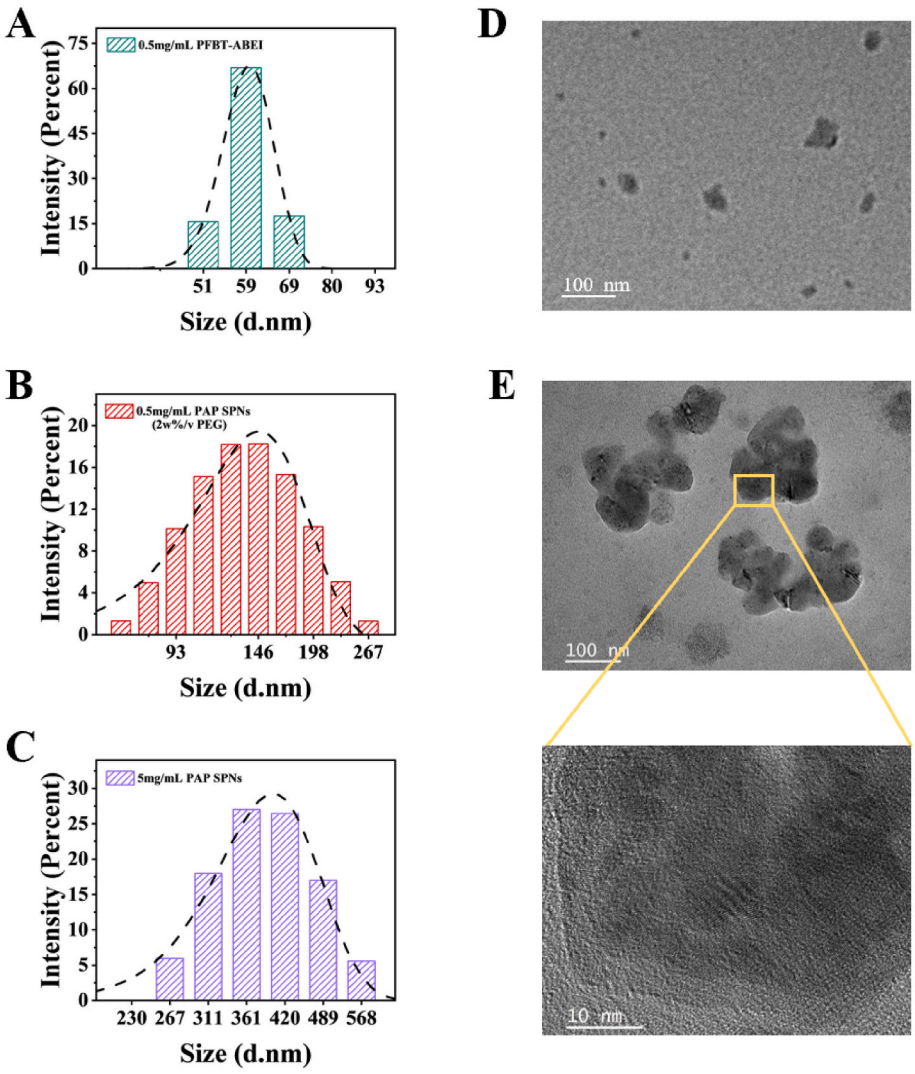

Fig. 2. (A–C) Size distribution of measured by DLS, and (D–F) TEM images of 0.5 mg/mL PFBT-ABEI, 0.5 mg/mL PAP SPNs.

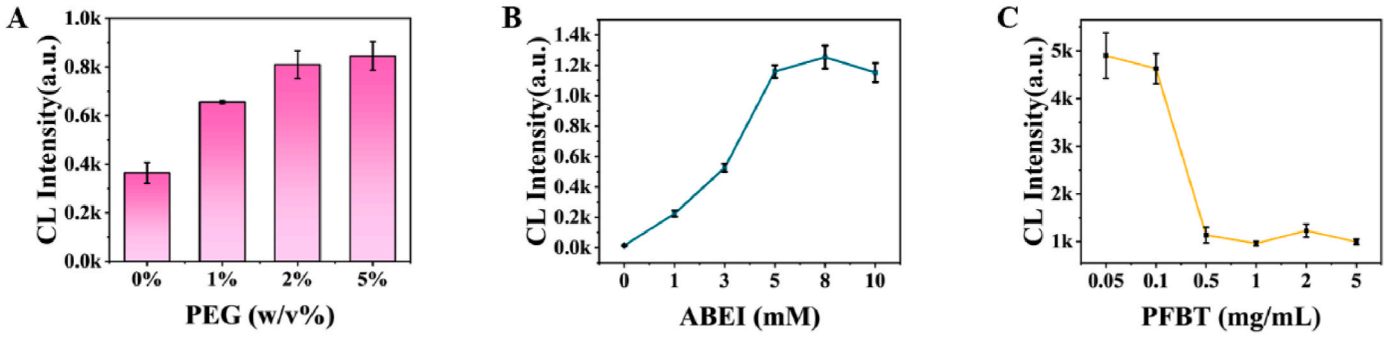

Fig. 3. Optimization of raw material concentration: (A) PEG, (B) ABEI, (C) PFBT.

encapsulated by PEG long chains and formed stable aggregates, which greatly reduced the probability of discrete random collisions and stabilizes the intramolecular CRET efficiency; in addition, the molecular dynamics behavior is transformed from a free diffusion to a state of restricted motion, and the spatial site-disturbance effect leads to an optimal equilibrium in the collision frequency. This greatly increases the stability of the experimental results and the reproducibility of the experimental operation.

The CL intensity of each component under a 550 bandpass filter is shown in Fig. S4. Based on the comprehensive consideration of performance and practicality, 2 w/v% PEG, 5 mM ABEI and 0.5 mg/mL PFBT were finally selected as the optimal feeding conditions.

2.3. Design and optimization of an CRET

In order to achieve CRET, it is necessary that the CL emission spectrum of the donor matches the absorption spectrum of the acceptor. Meanwhile, in accordance with the principle of CRET, the spatial

distance between donor and acceptor must be close enough [16,17]. The photophysical properties of ABEI, PFBT, PFBT-COOH, and PAP SPNs have been measured. Firstly, the spectral overlap of the absorption spectrum of PFBT-COOH and the CL emission spectrum of ABEI have been checked. As shown in Fig. 4A, PFBT exhibits two distinct absorption bands. The first range of band is between 300 nm and 400 nm, and the second is between 400 nm and 500 nm. The CL emission bands of ABEI ranged from 400 nm to 600 nm which considerably overlapped with the second range of PFBT absorption bands. A substantial overlap in the spectra of the two entities is observed, which allows for effective CRET. The UV–Vis absorption spectra (Fig. 4B) showed that both PFBT-COOH and PAP SPNs in water solution exhibit two absorption peaks. The first peak of PAP SPNs showed an obviously blue shift and higher absorbance compared with the first peak of PFBT-COOH. The second peak of PAP SPNs showed lower absorbance compared with PFBT-COOH at 470 nm. A comparison of the excitation and emission spectra between PFBT-ABEI and PAP SPNs, a significant discrepancy has been observed in the excitation spectra of them, and both reveal significant Stokes shift of approximately 100 nm (Fig. 4C and D).

The results of the measure of the spectra demonstrated that ABEI molecules with chemiluminescence ability could be function as an energy donor, which could emit blue light around 470 nm when oxidized and transfer energy from their excited state to the PFBT as acceptor. The main chain PFBT fluorophore, as an energy acceptor, could be excited by light around 470 nm to emit yellow fluorescence around 578 nm. Therefore, these experimental results demonstrate that ABEI and PFBT have successfully achieved CRET.

2.4. Principle for H_2O_2 detection

ABEI, as a potent chemiluminescent substrate, usually exists as a dipole ion (amphoteric ion) in neutral solution [32,33]. In alkaline solutions, it is transformed into a divalent negative ion and can be oxidized by oxygen molecules to intermediates capable of producing chemiluminescence [34]. In the presence of an oxidizing agent, ABEI is converted to an excited state, which subsequently decays back to the ground state and emits chemiluminescence [24,35]. Due to the small molecules have relatively high mobility and diffusivity in solution, covalent bonds were used to anchor ABEI groups to the surface of PFBT nanoparticles to restrict their spatial orientation and distribution.

Therefore, the chemiluminescence mechanism of this system is proposed as follows (Fig. 5A): HRP catalyzes the decomposition of H_2O_2 under alkaline conditions to generate a large number of highly reactive oxygen radicals, which not only accelerate the PFBT-ABEI negative ions to produce radicals $[PFBT\text{-}ABEI]^{\cdot}$, but also continue to react with dissolved oxygen to generate •OH, and $[PFBT\text{-}ABEI]^{\cdot}$ is further oxidized by •OH to generate [PFBT-ABEI]* to form the excited state of the luminophore, and the excited state of the luminophore returns to the ground state through the decay process of radiative and non-radiative leaps to produce strong CL emission [24,32–35].

As ROS play a pivotal role in this system, the identification and quantification of oxygen radical active species is imperative to elucidate the intramolecular CRET mechanism. Thus, a series of quenching assays were designed to compare the CL intensity by adding different ROS scavengers, in order to identify the major radical active species in this system. By using thiourea, superoxide dismutase (SOD) and L-histidine as specific scavengers of •OH, $O_2^{\bullet-}$ and $^1O_2$ [36–38], respectively, the present study systematically explored the above three species of ROS in the CRET reactions between H_2O_2 and PAP SPNs specific involvement mechanisms (Fig. 5B). The experimental results showed that the addition of thiourea significantly suppressed the CL intensity of the reaction, proving that •OH played a key role in the reaction. But SOD and L-histidine did not cause significant changes in the CL intensity and had relatively little effect on the CL intensity, indicating that the contribution of $O_2^{\bullet-}$ and $^1O_2$ was more limited.

2.5. Optimization of experimental conditions

The reaction conditions of PAP SPNs were systematically optimized for achieving high catalytic enhancement of CRET efficiency and increased CL intensity with extended chemiluminescence duration. In order to attain higher CL intensity, the parameters of the reactive system

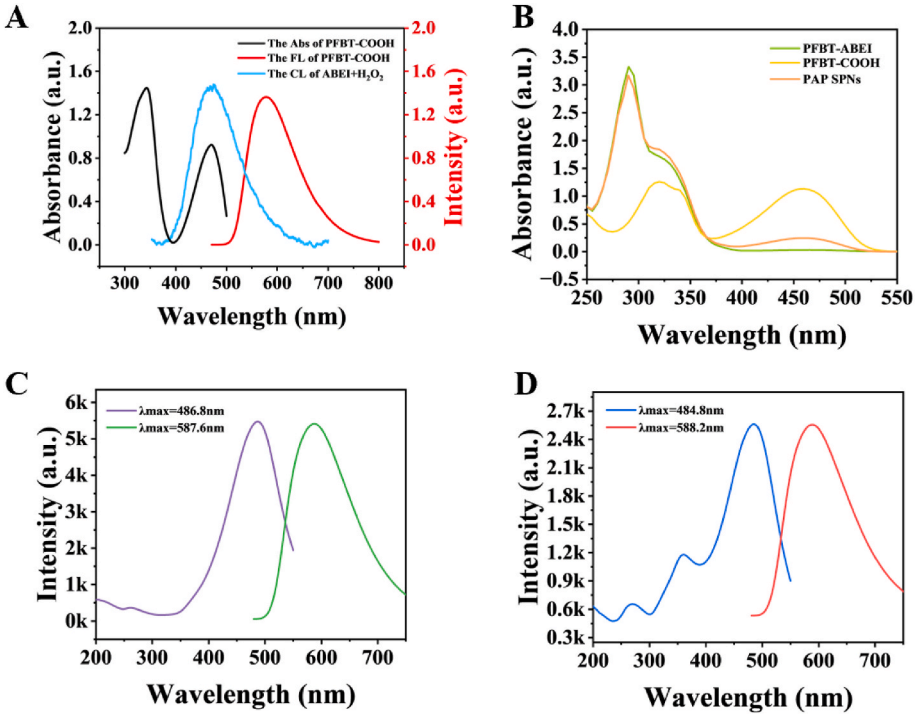

Fig. 4. (A) Absorption and emission spectra of PFBT-COOH (λex = 470 nm), and chemiluminescence spectra of ABEI. (B) UV–visible spectra of PFBT-COOH and PAP SPNs. Excitation and emission spectra of (C) PFBT-ABEI, (D) PAP SPNs.

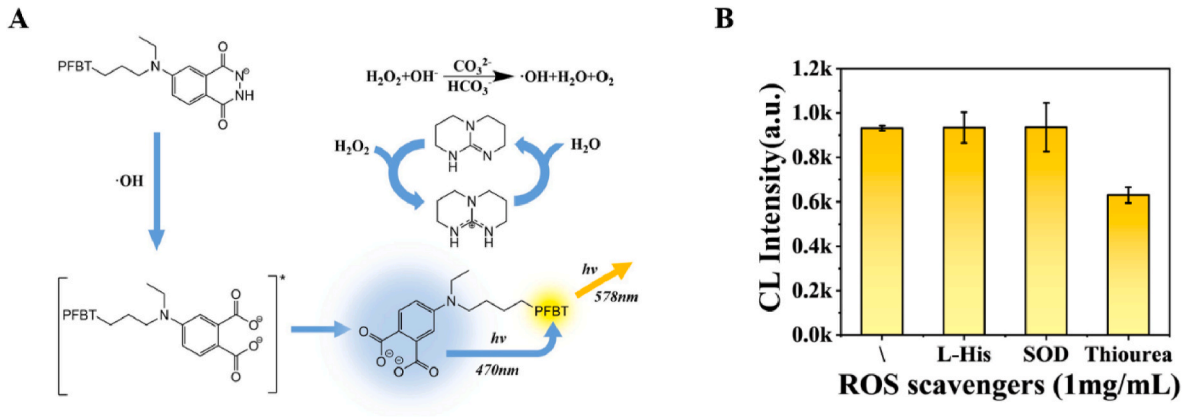

Fig. 5. (A) Chemiluminescent mechanism of PAP SPNs. (B) Influence of different ROS scavengers (1 mg/mL).

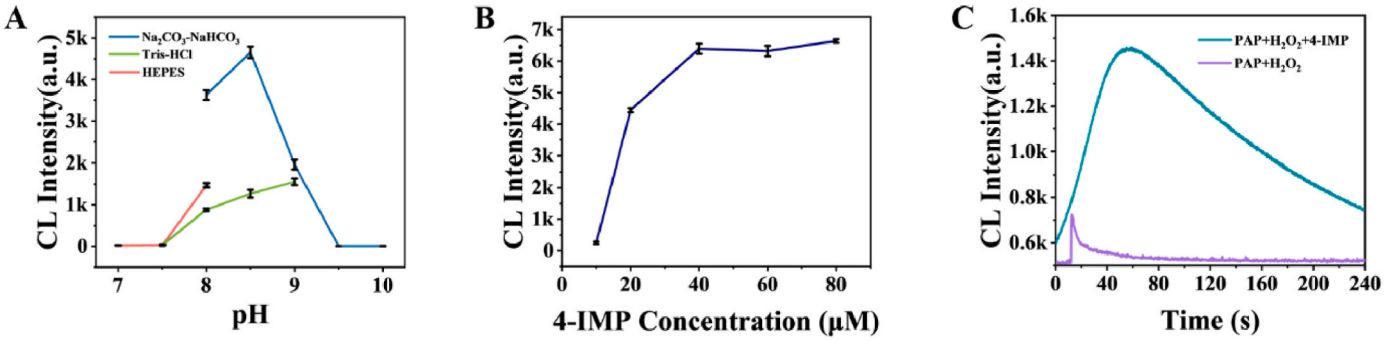

Fig. 6. Influence of (A) different buffer solution, (B) 4-IMP concentration. (C) Chemiluminescence dynamic profile of PAP SPNs and H_2O_2 with/without 4-IMP (40 μM).

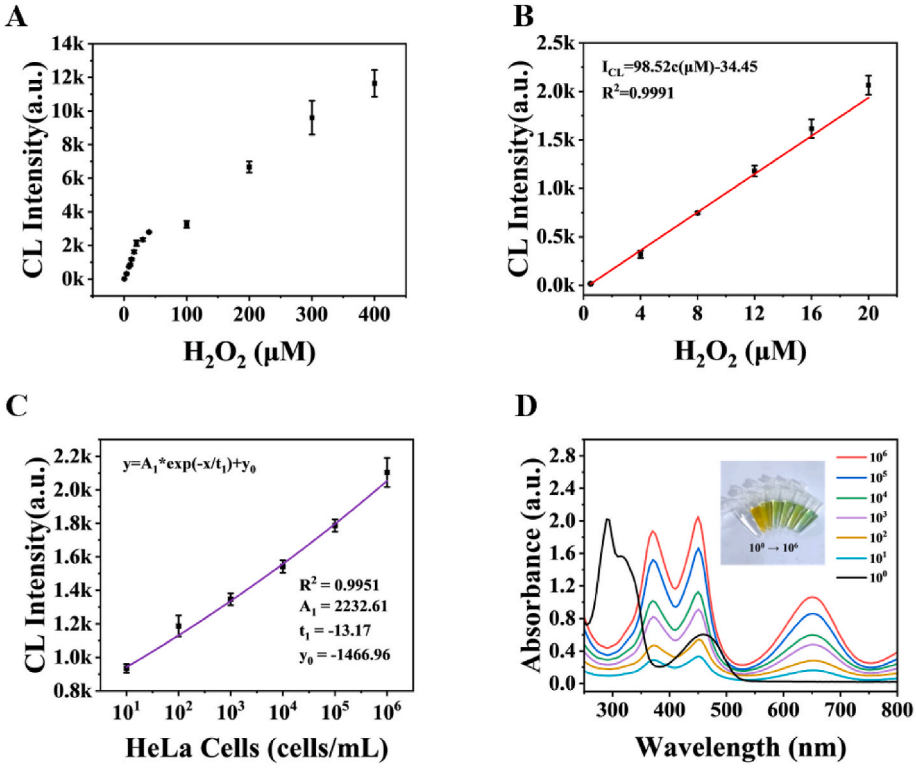

Fig. 7. (A) Detection range. (B) Linear relationship between the CL intensity and the concentration of H_2O_2 in the low concentration range. (C) Chemiluminescence intensities quantitative data and correlation fitting curve of HeLa cells treated with PAP SPNs. (D) Colorimetric TMB assay indicates the H_2O_2 yield of HeLa cells at different orders from 10^0 to 10^6 cells/mL and uw-vis absorption spectra.

were optimized for the detection of H_2O_2. Although temperature has a significant effect on the kinetics of enzyme reactions, we chose room temperature as the experimental condition for convenience of practical application and accuracy of experimental results. It is common knowledge that alkaline conditions are conducive to luminol and its analogues to generate more excited state products and increase its reactivity. Comparative analysis of CL intensity among 3 buffer systems (Na_2CO_3–$NaHCO_3$, Tris-HCl, and HEPES) across different pH values revealed that the Na_2CO_3–$NaHCO_3$ buffer at pH 8.5 yielded the most intense CL intensity (Fig. 6A).

It has been demonstrated that the addition of the 4-imp enhancer resulted in a substantial enhancement of the CL intensity [39]. As the concentration of 4-IMP increased, the CL intensity firstly increased significantly, and then its trend gradually moderated, and finally tended to a relatively stable state without obvious fluctuations (Fig. 6B). The CL intensity reached at least twofold that of the enhancer-free state, and the duration of the chemiluminescence was observed to increase sixfold compared with enhancer-free state (Fig. 6C). When the concentration of 4-IMP in the system was 40 μM, the CL intensity of the system was the maximum. However, as the HRP concentration gradually increased, the CL intensity continued to rise and with no indication of moderation. To sum up, 3 mg/L HRP (Fig. S5), 40 μM 4-IMP as well 0.1 M pH = 8.5 Na_2CO_3–$NaHCO_3$ were chosen by taking the CL intensity of H_2O_2 and PAP SPNs into consideration.

2.6. Determination of H_2O_2

The HRP-catalyzed PAP SPNs CRET reaction system for the detection of H_2O_2 was further investigated under optimal conditions. CL intensity showed a linear response to H_2O_2 concentration. According to Fig. 7A, the low concentration interval 0.5–20 μM was selected to establish the linear relationship between CL intensity and H_2O_2 concentration (Fig. 7B), and the linear regression equation was I_{CL} = 98.52c(μM)-34.45, with a correlation coefficient of 0.9991. The calculated limit of detection (LOD) was 33.88 nM (3σ/k, Table S1). The selectivity ability of this system was tested (Fig. S6), there were no remarkable CL signals after the treatment with other ROS/RNS or biological interferents alone. Although ClO^- can excite PAP SPNs, the CL of the HRP-H_2O_2 system is much larger than that of ClO^-.

A comparison of linear range and detection limit for PAP SPNs with other ROS detection by SPNs reported in literature are summarized in Table 1. The data demonstrate the analytical parameters of PAP SPNs is comparable or better than previous studies and is essentially lower than other FL, ECL and CL probes. It is indisputable the outstanding strengths of the CRET-based enzymatic H_2O_2 detection system are its super-low detection limit, excellent selectivity and sensitivity. Compared with FL and ECL, CL does not require an exogenous excitation source, which fundamentally eliminates light scattering and autofluorescence interference, and avoids photobleaching and excitation/emission spectral overlap, which are common in FL technology [27,40]. At the same time, CL overcomes the dependence of ECL on complex electrode systems and the technical challenge of potential regulation, thus obtaining a lower detection limit, which is more suitable for the dynamic monitoring of ROS in deep tissues.

Table 1
Comparison with previously reported methods for H_2O_2 detection.

Method	Materials	Analyte (ROS)	Linear range	LOD	Reference
CL	PFO@CPPO@Hemin	H_2O_2	50–500 μM	0.25 μM	[41]
CL	SPN-PFPV	H_2O_2	8 nM-10 μM	–	[40]
CL	PFV-L@PEG-FA-NPs	$^1O_2$	1–11 μM	–	[4]
ECL	ABEI-functionalized Pdots	H_2O_2	10–200 μM	3.3 μM	[42]
FL	$PFOBT_{36}SeTBT_x$ Pdots	ClO^-	50–250 μM	0.5 μM	[22]
PL and ECL	Ir-Fc	HOCl	5–40 μM	93.3 nM	[43]
CL	PAP SPNs	H_2O_2	0.5–20 μM	33.88 nM	This work

2.7. Determination of H_2O_2 in HeLa cells

The cytotoxicity of PAP SPNs in HeLa cells was evaluated by CCK8 assay, and the results showed that the material has good biocompatibility (Fig. S7). Since the chemiluminescence reaction of ABEI needs to be performed under alkaline conditions, an environment unsuitable for HeLa cell survival, this method is only suitable for cell lysate detection, providing an in vitro rapid screening solution for diseased tissues. We further carried out the assay using HeLa cells as actual samples, and the results showed that CL intensity was positively correlated with the cell number, and after normalization, the signal was significantly enhanced with the increase of cell number (Fig. 7C). When the number of cells was taken as logarithmic, a linear correlation was obtained in the concentration range of 1.34×10^1 cells/mL to 1.34×10^6 cells/mL with an R^2 of 0.9951. The experimental results showed a good linear relationship between different cell number levels and CL intensity, a finding that confirms the high sensitivity and reliability of this CRET assay system in quantifying HeLa cell number. Furthermore, to corroborate the reliability of the experimental system, parallel validation was performed using the 3,3′,5,5′-tetramethylbenzidine (TMB) chromogenic assay (Fig. 7D). The experimental results showed that with the increase of cell density, the TMB chromogenic reaction showed significant concentration-dependent characteristics, the color of the reaction system was gradually deepened, and the absorbance showed an increasing trend. The feasibility of PAP SPNs for the detection of H_2O_2 content in cell lysate was confirmed by the double validation of the above two experiments.

The study validated the highly specific response mechanism of PAP SPNs to HRP-H_2O_2 through systematic experiments, confirming the high sensitivity and excellent selectivity of the assay, and further validating the potential of the system in detecting and quantifying H_2O_2 levels in cancer cells. These results not only provide a new technological tool for the early disease diagnosis, but also offer new ideas for the development of chemiluminescence-based high-sensitivity biosensors. In the future, this technology can be further optimized and applied to the real-time detection and ultrasensitive imaging of ROS in living organisms, providing a powerful tool to study the mechanism of CRET in the development of diseases, which has significant clinical application prospects and extensive biological research value.

3. Conclusion

In this study, we successfully designed and developed a novel semiconducting polymer nanoparticle for the detection of H_2O_2 based on CRET. The system was constructed by exploiting the highly efficient chemiluminescence reaction between ABEI and hydrogen peroxide (H_2O_2)-horseradish peroxidase (HRP), as well as the intramolecular CRET mechanism between ABEI and PFBT. The experimental results showed that the developed sensor exhibited excellent linear response characteristics in the H_2O_2 concentration range of 0.5–20 μM, along with good selectivity and sensitivity. In addition, we explored the optimal feeding ratio for synthesizing PAP SPNs, which effectively improved the efficiency of CRET, enhanced CL intensity, and successfully overcame the major limitations of conventional chemiluminescent systems such as low emission intensity and scintillation-type emission. This breakthrough opens up new possibilities for the application of chemiluminescence imaging in biological organisms, especially for real-time monitoring of biomolecular dynamics.

CRediT authorship contribution statement

Ximin Mai: Writing – review & editing, Writing – original draft, Validation, Investigation, Formal analysis, Data curation. **Jiahui Li:** Investigation, Formal analysis. **Pinyi Ma:** Writing – review & editing. **Daqian Song:** Writing – review & editing. **Qiang Fei:** Writing – review & editing, Funding acquisition, Conceptualization.

Declaration of competing interest

The authors declare that they have no known competing financial interests or personal relationships that could have appeared to influence the work reported in this paper.

Acknowledgements

This work was supported by the Natural Science Foundation of Jilin Province, China (No. 20210101118JC).

Appendix A. Supplementary data

Supplementary data to this article can be found online at https://doi.org/10.1016/j.talanta.2025.128449.

Data availability

Data will be made available on request.

References

[1] S. Zhang, H. Yuan, S. Sun, C. Qin, Q. Qiu, Y. Feng, Y. Liu, Y. Li, L. Xu, Y. Ying, J. Qi, Y. Wang, Self-Illuminating NIR-II chemiluminescence nanosensor for in vivo tracking H_2O_2 fluctuation, Adv. Sci. 10 (23) (2023).
[2] B. Kalyanaraman, G. Cheng, M. Hardy, O. Ouari, B. Bennett, J. Zielonka, Teaching the basics of reactive oxygen species and their relevance to cancer biology: mitochondrial reactive oxygen species detection, redox signaling, and targeted therapies, Redox Biol. 15 (2018) 347–362.
[3] R.E. Morty, C.E.A. Souza, D. Maitra, G.M. Saed, M.P. Diamond, A.A. Moura, S. Pennathur, H.M. Abu-Soud, Hypochlorous acid-induced heme degradation from lactoperoxidase as a novel mechanism of free iron release and tissue injury in inflammatory diseases, PLoS One 6 (11) (2011).
[4] L. Li, X. Zhang, Y. Ren, Q. Yuan, Y. Wang, B. Bao, M. Li, Y. Tang, Chemiluminescent conjugated polymer nanoparticles for deep-tissue inflammation imaging and photodynamic therapy of cancer, J. Am. Chem. Soc. 146 (9) (2024) 5927–5939.
[5] S. Lelieveld, J. Wilson, E. Dovrou, A. Mishra, P.S.J. Lakey, M. Shiraiwa, U. Pöschl, T. Berkemeier, Hydroxyl radical production by air pollutants in epithelial lining fluid governed by interconversion and scavenging of reactive oxygen species, Environmental Science & Technology 55 (20) (2021) 14069–14079.
[6] S.J. Forrester, D.S. Kikuchi, M.S. Hernandes, Q. Xu, K.K. Griendling, Reactive oxygen species in metabolic and inflammatory signaling, Circ. Res. 122 (6) (2018) 877–902.
[7] J. Zuo, Z. Zhang, M. Li, Y. Yang, B. Zheng, P. Wang, C. Huang, S. Zhou, The crosstalk between reactive oxygen species and noncoding RNAs: from cancer code to drug role, Mol. Cancer 21 (1) (2022).
[8] H. Yang, R.M. Villani, H. Wang, M.J. Simpson, M.S. Roberts, M. Tang, X. Liang, The role of cellular reactive oxygen species in cancer chemotherapy, J. Exp. Clin. Cancer Res. 37 (1) (2018).
[9] I.I.C. Chio, D.A. Tuveson, ROS in cancer: the burning question, Trends Mol. Med. 23 (5) (2017) 411–429.
[10] F.L. Sarmiento-Salinas, A. Perez-Gonzalez, A. Acosta-Casique, A. Ix-Ballote, A. Diaz, S. Treviño, N.H. Rosas-Murrieta, L. Millán-Perez-Peña, P. Maycotte, Reactive oxygen species: role in carcinogenesis, cancer cell signaling and tumor progression, Life Sci. 284 (2021).
[11] J. Pan, W. Li, M. Wang, C. Peng, J. Dong, Q. Zhou, F. Xia, Conjugated polymer for NIR-II phototheranostics toward tumor, Chem. Mater. 36 (24) (2024) 11721–11737.
[12] A.B. Solea, M.D. Ward, A chemiluminescent lantern: a coordination cage catalysed oxidation of luminol followed by chemiluminescence resonance energy-transfer, Dalton Trans. (2003) 52 (14) (2023) 4456–4461.
[13] H. Li, Y. Sun, Y. Li, J. Du, Alkaline phosphatase activity assay with luminescent metal organic frameworks-based chemiluminescent resonance energy transfer platform, Microchem. J. 160 (2021).
[14] Y. Sun, X. Xu, Y. Zhao, H. Tan, Y. Li, J. Du, Luminescent metal organic frameworks–based chemiluminescence resonance energy transfer platform for turn–on detection of fluoride ion, Talanta 209 (2020).
[15] J. Chen, H. Qiu, S. Zhao, Fabrication of chemiluminescence resonance energy transfer platform based on nanomaterial and its application in optical sensing, biological imaging and photodynamic therapy, TrAC, Trends Anal. Chem. 122 (2020).
[16] Y. Yan, X.-y. Wang, X. Hai, W. Song, C. Ding, J. Cao, S. Bi, Chemiluminescence resonance energy transfer: from mechanisms to analytical applications, TrAC, Trends Anal. Chem. 123 (2020).
[17] J. Lou, X. Tang, H. Zhang, W. Guan, C. Lu, Chemiluminescence resonance energy transfer efficiency and donor–acceptor distance: from qualitative to quantitative, Angew. Chem. Int. Ed. 60 (23) (2021) 13029–13034.
[18] S. Bi, M. Chen, X. Jia, Y. Dong, A hot-spot-active magnetic graphene oxide substrate for microRNA detection based on cascaded chemiluminescence resonance energy transfer, Nanoscale 7 (8) (2015) 3745–3753.
[19] B.J. Jia, X. He, P.L. Cui, J.X. Liu, J.P. Wang, Detection of chloramphenicol in meat with a chemiluminescence resonance energy transfer platform based on molecularly imprinted graphene, Anal. Chim. Acta 1063 (2019) 136–143.
[20] S. Xu, X. Li, C. Li, J. Li, X. Zhang, P. Wu, X. Hou, In situ generation and consumption of H_2O_2 by Bienzyme–Quantum dots bioconjugates for improved chemiluminescence resonance energy transfer, Anal. Chem. 88 (12) (2016) 6418–6424.
[21] X. Liu, J. Li, T. Wen, Z. Li, X. Wang, M. Li, P. Ma, D. Song, Q. Fei, Copper ion ratio chemiluminescence probe based on chemiluminescence resonance energy transfer, Microchem. J. 187 (2023).
[22] L. Wu, I.C. Wu, C.C. DuFort, M.A. Carlson, X. Wu, L. Chen, C.-T. Kuo, Y. Qin, J. Yu, S.R. Hingorani, D.T. Chiu, Photostable ratiometric pdot probe for in vitro and in vivo imaging of hypochlorous acid, J. Am. Chem. Soc. 139 (20) (2017) 6911–6918.
[23] J. Du, Y. Wang, W. Zhang, Gold nanoparticles-based chemiluminescence resonance energy transfer for ultrasensitive detection of melamine, Spectrochim. Acta Mol. Biomol. Spectrosc. 149 (2015) 698–702.
[24] R. Freeman, X. Liu, I. Willner, Chemiluminescent and Chemiluminescence Resonance Energy Transfer (CRET) detection of DNA, metal ions, and aptamer–substrate complexes using Hemin/G-Quadruplexes and CdSe/ZnS quantum dots, J. Am. Chem. Soc. 133 (30) (2011) 11597–11604.
[25] Y. Jiang, J. McNeill, Light-Harvesting and amplified energy transfer in conjugated polymer nanoparticles, Chem. Rev. 117 (2) (2016) 838–859.
[26] H.-S. Peng, D.T. Chiu, Soft fluorescent nanomaterials for biological and biomedical imaging, Chem. Soc. Rev. 44 (14) (2015) 4699–4722.
[27] C. Wu, D.T. Chiu, Highly fluorescent semiconducting polymer dots for biology and medicine, Angew. Chem. Int. Ed. 52 (11) (2013) 3086–3109.
[28] L.R. MacFarlane, H. Shaikh, J.D. Garcia-Hernandez, M. Vespa, T. Fukui, I. Manners, Functional nanoparticles through π-conjugated polymer self-assembly, Nat. Rev. Mater. 6 (1) (2020) 7–26.
[29] J. Yu, Y. Rong, C.-T. Kuo, X.-H. Zhou, D.T. Chiu, Recent advances in the development of highly luminescent semiconducting polymer dots and nanoparticles for biological imaging and medicine, Anal. Chem. 89 (1) (2016) 42–56.
[30] X. Wang, Y. Xu, Q. Ou, W. Chen, W. van der Meer, G. Liu, Adsorption characteristics and mechanisms of water-soluble polymers (PVP and PEG) on kaolin and montmorillonite minerals, J. Hazard Mater. 466 (2024) 133592.
[31] U. Dahal, Z. Wang, E.E. Dormidontova, Hydration of spherical PEO-grafted gold nanoparticles: curvature and grafting density effect, Macromolecules 51 (15) (2018) 5950–5961.
[32] H. Wu, M. Zhao, J. Li, X. Zhou, T. Yang, D. Zhao, P. Liu, H. Ju, W. Cheng, S. Ding, Novel protease-free long-lasting chemiluminescence system based on the Dox-ABEI chimeric magnetic DNA hydrogel for ultrasensitive immunoassay, ACS Appl. Mater. Interfaces 12 (42) (2020) 47270–47277.
[33] X. Zhou, C. Fan, Q. Tian, C. Han, Z. Yin, Z. Dong, S. Bi, Trimetallic AuPtCo nanopolyhedrons with Peroxidase- and catalase-like catalytic activity for glow-type chemiluminescence bioanalysis, Anal. Chem. 94 (2) (2021) 847–855.
[34] F. Qu, J. Shu, S. Wang, M.A. Haghighatbin, H. Cui, Chemiluminescent nanogels as intensive and stable signal probes for fast immunoassay of SARS-CoV-2 nucleocapsid protein, Anal. Chem. 94 (49) (2022) 17073–17080.
[35] Y. Liu, W. Shen, H. Cui, Combined transition-Metal/Enzyme dual catalytic system for highly intensive glow-type chemiluminescence-functionalized $CaCO_3$ microspheres, Anal. Chem. 91 (16) (2019) 10614–10621.
[36] G.V. Buxton, C.L. Greenstock, W.P. Helman, A.B. Ross, Critical review of rate constants for reactions of hydrated electrons, hydrogen atoms and hydroxyl radicals (·OH/·O− in aqueous solution, J. Phys. Chem. Ref. Data 17 (2) (1988) 513–886.
[37] X. Xue, N. Xue, D. Ouyang, L. Yang, Y. Wang, H. Zhu, A. Aihemaiti, J. Yin, Biochar-based single-atom catalyst with Fe-N_3O-C configuration for efficient degradation of organic dyes by peroxymonosulfate activation, ACS Appl. Mater. Interfaces 49 (15) (2023) 57003–57014.
[38] A. Lyu, Y. Wang, H. Cui, Enhanced chemiluminescence under the nanoconfinement of covalent–organic frameworks and its application in sensitive detection of cancer biomarkers, Anal. Chem. 95 (20) (2023) 7914–7923.
[39] T. Eckle, L. Yang, M. Jin, P. Du, G. Chen, C. Zhang, J. Wang, F. Jin, H. Shao, Y. She, S. Wang, L. Zheng, J. Wang, Study on enhancement principle and stabilization for the Luminol-H_2O_2-HRP chemiluminescence system, PLoS One 10 (7) (2015).
[40] X. Zhen, C. Zhang, C. Xie, Q. Miao, K.L. Lim, K. Pu, Intraparticle energy level alignment of semiconducting polymer nanoparticles to amplify chemiluminescence for ultrasensitive in vivo imaging of reactive oxygen species, ACS Nano 10 (6) (2016) 6400–6409.
[41] Y. Wang, L. Shi, Z. Ye, K. Guan, L. Teng, J. Wu, X. Yin, G. Song, X.-B. Zhang, Reactive oxygen correlated chemiluminescent imaging of a semiconducting

polymer nanoplatform for monitoring chemodynamic therapy, Nano Lett. 20 (1) (2020) 176–183.

[42] Z. Wang, H. Guo, Z. Luo, Y. Duan, Y. Feng, Low-triggering-potential electrochemiluminescence from a luminol analogue functionalized semiconducting polymer dots for imaging detection of blood glucose, Anal. Chem. 94 (14) (2022) 5615–5623.

[43] F. Zhang, X. Liang, W. Zhang, Y.-L. Wang, H. Wang, Y.H. Mohammed, B. Song, R. Zhang, J. Yuan, A unique iridium(III) complex-based chemosensor for multi-signal detection and multi-channel imaging of hypochlorous acid in liver injury, Biosens. Bioelectron. 87 (2017) 1005–1011.